Inorg. Chem. **2009**, *48*, 4454−4461

Ferromagnetic and Antiferromagnetic Coupling of $[Ni(dmit)_2]^-$ Anion Layers Induced by $Cs^+_2(benzo[18]crown\text{-}6)_3$ Supramolecule

Tomoyuki Akutagawa,*,†,‡ Kozo Shitagami,‡ Masaki Aonuma,‡ Shin-ichiro Noro,†,‡ and Takayoshi Nakamura*,†,‡

Research Institute for Electronic Science, Hokkaido University, Sapporo 001-0020, Japan, and Graduate School of Environmental Science, Hokkaido University, Sapporo 060-0810, Japan

Received January 29, 2009

Sandwich-type $(Cs^+)_2$(benzo[18]crown-6)$_3$ and (Cs^+)(dibenzo[18]crown-6)$_2$ supramolecular cations were introduced as counterions of $[Ni(dmit)_2]^-$ ($dmit^{2-}$ = 2-thione-1,3-dithiole-4,5-dithiolate) anions to induce unique $[Ni(dmit)_2]^-$ anion ($S = 1/2$) arrangements and magnetic properties. The magnetic exchange energy (J) between the $[Ni(dmit)_2]^-$ anions was dependent on the mode of the intermolecular interactions. In the case of $(Cs^+)_2$(benzo[18]crown-6)$_3[Ni(dmit)_2]^-_2$ (**1**), the asymmetric arrangement of the $[Ni(dmit)_2]^-$ anions involved the coexistence of a π-dimer chain along with a two-dimensional layer via lateral S···S contacts, in which the magnetic properties of the π-dimer chain and the two-dimensional layer were characterized by antiferromagnetic ($J = -5.2$ K) and ferromagnetic coupling (Weiss temperature = +1.1 K), respectively. The unique $[Ni(dmit)_2]^-$ arrangements and magnetic behaviors for crystal **1** can be attributed to the asymmetrical benzo[18]crown-6. In the case of Cs^+(dibenzo[18]crown-6)$_2[Ni(dmit)_2]^-$ (**2**), however, the formation of the lateral $[Ni(dmit)_2]^-$ dimer via S···S contacts yielded antiferromagnetic coupling corresponding to the dimer model ($J = -25.5$ K).

Introduction

Various magnetic properties such as the ferromagnetic, antiferromagnetic, ferrimagnetic, and metamagnetic interactions have been realized by regulating the intermolecular magnetic exchange energy (J) within a molecular crystal.[1] The magnetic orderings are induced by long-range ferromagnetic ($J_F > 0$) or antiferromagnetic ($J_{AF} < 0$) spin coupling.[1] Although small negative J values are commonly observed for a majority of molecular crystals, the magnetic coupling can be manipulated by regulating the anisotropic intermolecular interactions.[2] A highly effective method in controlling the molecular arrangements involves the simultaneous control of the $J_F > 0$ and $J_{AF} < 0$ interactions, which affect the independent magnetic responses for the changes in outer magnetic fields or temperatures.[3] It has been proposed that the interfacial junction between the magnetic domain of $J_F > 0$ and $J_{AF} < 0$ can appear as a gigantic magneto resistance and spin valves.[4] Inorganic compounds such as $Ca_{0.9}Pr_{0.1}MnO_3$ and $GdFe_6Mn_6$ have exhibited crossover of magnetic coupling from $J_F > 0$ to $J_{AF} < 0$ by

* To whom correspondence should be addressed. E-mail: takuta@es.hokudai.ac.jp (T.A.), tnaka@es.hokudai.ac.jp (T.N.). Phone: +81-11-706-9418. Fax: +81-11-706-9420.

† Research Institute for Electronic Science.

‡ Graduate School of Environmental Science.

(1) Kahn, O. *Molecular Magnetism*; VCH, Weinheim, 1993. (b) Carlin, R. L. *Magnetochemistry*; Springer-Verlag: Heidelberg, 1986. (c) Miller, J. S.; Epstein, A. J. *Angew. Chem., Int. Ed. Engl.* **1994**, *33*, 385. (d) *Magnetism: Molecules to Materials*; Miller, J. S.; Drillon, M., Eds.; Wiley-VCH: Weinheim, 2001.

(2) (a) Heutz, S.; Mitra, C.; Wu, W.; Fisher, A. J.; Kerridge, A.; Stoneham, M.; Harker, T. H.; Gardener, J.; Tseng, H.-H.; Jones, T. S.; Renner, C.; Aeppli, G. *Adv. Mater.* **2007**, *19*, 3618. (b) Bogani, L.; Sangregorio, C.; Sessoli, R.; Gatteschi, D. *Angew. Chem., Int. Ed.* **2005**, *44*, 5817. (c) Noveron, J. C.; Lah, M. S.; Del, S.; Rico, E.; Arif, A. M.; Miller, J. S.; Stang, P. J. *J. Am. Chem. Soc.* **2002**, *124*, 6613. (d) Coronado, E.; Clemente-Leon, M.; Galan-Mascaros, J. R.; Gimenez-Saiz, C.; Gomez-Garcia, C. J.; Martinez-Ferrero, E. *Dalton Trans.* **2000**, 395.

(3) (a) Nath, R.; Tsirlin, A. A.; Kaul, E. E.; Baenitz, M.; Buttgen, N.; Geibel, C.; Rosner, H. *Phys. Rev. B* **2008**, *78*, 024418. (b) Grazioli, C.; Alfe, D.; Krishnakumar, S. R.; Sen Gupta, S.; Veronese, M.; Turchini, S.; Bonini, N.; Dal Corso, A.; Sarma, D. D.; Baroni, S.; Carbone, C. *Phys. Rev. Lett.* **2005**, *95*, 117201. (c) Boskovic, C.; Bircher, R.; Tregenna, P.; Philip, L. W.; Guedel, H. U.; Paulsen, C.; Wernsdorfer, W.; Barra, A.; Khatsko, E.; Neels, A.; Stoeckli-Evans, H. *J. Am. Chem. Soc.* **2003**, *125*, 14046.

(4) (a) Salafranca, J.; Calderon, M. J.; Brey, L. *Phys. Rev. B* **2008**, *77*, 014441. (b) Niebieskikwiat, D.; Hueso, L. E.; Salamon, M. B.; Mathur, N. D. *J. Appl. Phys.* **2006**, *99*, 08C903. (c) Li, M. H.; Yu, G. H.; Jiang, H. W.; Cai, J. W.; Lai, W. Y.; Zhu, F. W. *J. Appl. Phys.* **2002**, *92*, 2620. (d) Nolting, F.; Scholl, A.; Stohr, J.; Seo, J. W.; Fompeyrine, J.; Slegwart, H.; Locquet, J.-P.; Anders, S.; Luning, J.; Fullerton, E. E.; Toney, M. F.; Scheinfein, M. R.; Padmore, H. A. *Nature (London)* **2000**, *405*, 767.

10.1021/ic9001847 CCC: $40.75
Published on Web 03/27/2009

applying a magnetic field and/or sweeping the temperature.[5] For these materials, different crystallographic sites of the d- and f-spins can be designed for the simultaneous appearance of J_F and J_{AF}. In addition, the relatively strong magnetic exchange interactions between the spin sites resulted in the strong coupling between J_F and J_{AF}. Although novel magnetic systems that simultaneously possess J_F and J_{AF} interactions within a molecular crystal have the potential to offer novel multifunctional magnetic materials, their weak magnetic coupling, relative to inorganic compounds, is disadvantageous. Metal-organic coordination polymers such as Cu(II)-polychlorotriphenylmethyl radical and Gd(III)-isonicotinic acid have served as successful examples of simultaneous J_F and J_{AF} interactions.[5c,d] Antiferromagnetic ordering (T_N = 3.4 K) via ferromagnetic coupling has been observed for molecular crystals of segregated-stack charge-transfer complexes between (1,3,2-benzodithiazolyl$^+$) and $[Ni(mnt)_2]^-$ (mnt^{2-} = maleonitriledithiolate).[6] It has been shown that the negative spin density of the 1,3,2-benzodithiazolyl cation plays an important role in the superexchange mechanisms between the cations and anions.[7] Because of the anisotropic molecular structures and the structural flexibility within the molecular structure, such molecular crystals can form unique intermolecular magnetic interactions, and therefore, allow the control the magnetic interactions of the molecular crystals.

Recently, a variety of electrically and magnetically active molecular materials have been prepared using the $[Ni(dmit)_2]$ ($dmit^{2-}$ = 2-thioxo-1,3-dithiole-4,5-dithiolate) anion,[8] which can serve as a source of conducting electrons and/or localized $S = 1/2$ spins, according to the oxidation states. The monovalent $[Ni(dmit)_2]^-$ anion bearing one $S = 1/2$ spin has been effectively utilized in developing magnetic materials with various magnetic properties that arise from diverse modes of intermolecular interactions.[9,11] As shown in Figure 1, the one, two, and three-dimensional magnetic exchange pathways within the crystals are defined by the following arrangements of the among the $[Ni(dmit)_2]$ anions: (a) π-stacking, (b, c) lateral S···S contacts along the long or short axes, and (d) the orthogonal π-overlap.[8−11] A frequently observed intermolecular interaction mode involves the π-stacking dimer (Figure 1a), which exhibits magnetism that is consistent with that of the dimer model with $J_{AF} < 0$.

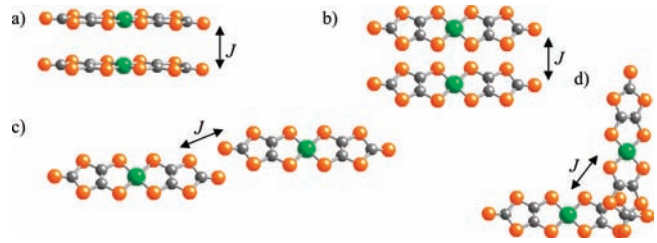

Figure 1. Intermolecular interaction modes between the $[Ni(dmit)_2]^-$ anions: (a) π-dimer, (b) lateral S···S interactions along the short axis of the $[Ni(dmit)_2]^-$ anions, (c) lateral S···S interactions along the long axis of the $[Ni(dmit)_2]^-$ anions, and (d) orthogonal π-overlap.

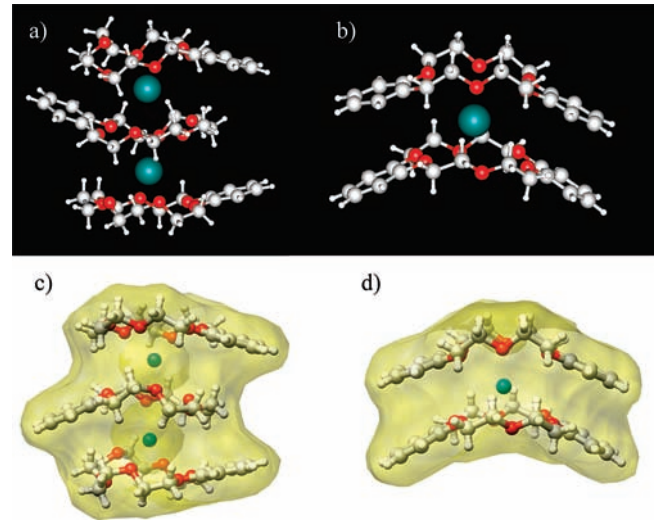

Figure 2. Supramolecular cations of $Cs^+{}_2$(B[18]crown-6)$_3$ (a, c) and Cs^+(DB[18]crown-6)$_2$ (b, d) for salts **1** and **2**. All structural units are crystallographically independent to each other. Surface potentials for the cation structures were drawn to show the overall shapes of supramolecular assemblies.

We have previously reported on the magnetic properties of $[Ni(dmit)_2]^-$ crystals that feature supramolecular cations composed of inorganic or organic cations and crown ether derivatives.[11] Such supramolecular cations, depending on their size and shape, have been shown to induce diverse $[Ni(dmit)_2]^-$ anion arrangements within the crystals. For example, the K^+([18]crown-6) cation yielded a one-dimensional antiferromagnetic Heisenberg chain of the $[Ni(dmit)_2]^-$ anions, whereas the (anilinium$^+$)([18]crown-

(5) (a) Savosta, M. M.; Novák, P.; Maryško, M.; Jirák, Z.; Hejtmánek, J.; Englich, J.; Kohout, J.; Martin, C.; Raveau, B. *Phys. Rev. B* **2000**, *62*, 9352. (b) Piqué, C.; Blanco, J. A.; Burriel, R.; Abad, E.; Artigas, M.; Fernández-Díaz, M. T. *Phys. Rev. B* **2007**, *75*, 224424. (c) Luo, F.; Hu, D.; Xue, L.; Che, Y.; Zheng, J. *Cryst. Growth Des.* **2007**, *5*, 851. (d) Maspoch, D.; Domingo, N.; Ruiz-Molina, D.; Wurst, K.; Hernández, J.-M.; Vaugham, G.; Rovira, C.; Lloret, F.; Tejada, J.; Veciana, J. *Chem. Commun.* **2005**, 5035.

(6) Umezono, Y.; Fujita, W.; Awaga, K. *Chem. Phys. Lett.* **2005**, *209*, 139.

(7) McConnel, H. M. *J. Chem. Phys.* **1963**, *39*, 1910.

(8) (a) Cassoux, P.; Valade, L.; Kobayashi, H.; Kobayashi, A.; Clark, R. A.; Underhill, A. E. *Coord. Chem. Rev.* **1991**, *110*, 115. (b) Pullen, A. E.; Olk, R.-K. *Coord. Chem. Rev.* **1999**, *188*, 211. (c) Faulmann, C.; Cassoux, P. *Prog. Inorg. Chem.* **2004**, *52*, 399. (d) Kato, R. *Chem. Rev.* **2004**, *104*, 5319.

(9) (a) Broderick, W. E.; Thompson, J. A.; Godfrey, M. R.; Sabat, M.; Hoffman, B. M. *J. Am. Chem. Soc.* **1989**, *111*, 7657. (b) Coomber, A. T.; Beljonne, D.; Friend, R. H.; Brédas, J. J.; Charlton, A.; Robertson, N.; Underhill, A. E.; Kurmoo, M.; Day, P. *Nature (London)* **1996**, *380*, 144.

(10) (a) Kobayashi, A.; Sato, A.; Kobayashi, H. *J. Solid State Chem.* **1999**, *145*, 564. (b) Kato, R.; Kobayashi, H.; Kim, H.; Kobayashi, A. *Chem. Lett.* **1988**, 865.

(11) (a) Takamatsu, N.; Akutagawa, T.; Hasegawa, T.; Nakamura, T.; Inabe, T.; Fujita, W.; Awaga, K. *Inorg. Chem.* **2000**, *39*, 870. (b) Akutagawa, T.; Nishihara, S.; Takamatsu, N.; Hasegawa, T.; Nakamura, T.; Inabe, T. *J. Phys. Chem. B* **2000**, *104*, 5871. (c) Cronin, L.; Clark, S. J.; Parsons, S.; Nakamura, T.; Robertson, N. *Dalton Trans.* **2001**, 1347. (d) Akutagawa, T.; Hashimoto, A.; Nishihara, S.; Hasegawa, T.; Nakamura, T. *J. Phys. Chem. B.* **2003**, *107*, 66. (e) Akutagawa, T.; Matsuura, K.; Hashimoto, A.; Nakamura, T. *Inorg. Chem.* **2005**, *44*, 4454. (f) Akutagawa, T.; Shitagami, K.; Nishihara, S.; Takeda, S.; Hasegawa, T.; Nakamura, T.; Hosokoshi, Y.; Inoue, K.; Ikeuchi, S.; Miyazaki, Y.; Saito, K. *J. Am. Chem. Soc.* **2005**, *127*, 4397. (g) Sato, D.; Akutagawa, T.; Takeda, S.; Noro, S.; Nakamura, T. *Inorg. Chem.* **2007**, *46*, 363. (h) Nishihara, S.; Akutagawa, T.; Sato, D.; Takeda, S.; Noro, S.; Nakamura, T. *Chem.—Asian J.* **2007**, *2*, 1983. (i) Akutagawa, T.; Sato, D.; Koshinaka, H.; Aonuma, M.; Noro, S.; Takeda, S.; Nakamura, T. *Inorg. Chem.* **2008**, *47*, 5951. (j) Akutagawa, T.; Nakamura, T. *Dalton Trans.* **2008**, 6335.

Scheme 1. Molecular Structures of Benzo[18]crown-6 (B[18]crown-6), Dibenzo[18]crown-6 (DB[18]crown-6), and $[Ni(dmit)_2]^-$ Anion

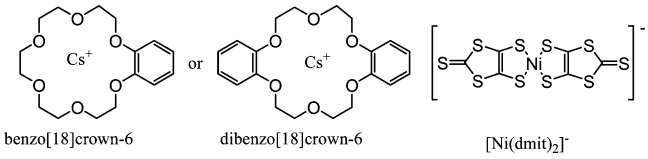

6) cation resulted in a two-legged ladder chain of the anions.[11] Although a large number of $[Ni(dmit)_2]^-$ anion arrangements have been achieved using such supramolecular cations, a majority of the magnetic coupling between the $[Ni(dmit)_2]^-$ anions were characterized by negative J_{AF} values. However, ferromagnetic interactions with a Weiss temperature of +0.9 K[11i] was observed for the crystals formed using (anilinium$^+$)(dicyclohexano[18]crown-6), in which the $[Ni(dmit)_2]^-$ anions formed a uniform lateral S···S chain along the short axis of the $[Ni(dmit)_2]^-$ anions, as shown in Figure 1b. In contrast to the π-stacking (Figure 1a) and uniform lateral S···S chain along the long axis of $[Ni(dmit)_2]^-$ anions (Figure 1c) modes, which yield $J_{AF} < 0$ interactions, the uniform anion arrangement along the short axis of $[Ni(dmit)_2]^-$ can generate $J_F > 0$ interactions within the crystals.

Our investigations on magnetic $[Ni(dmit)_2]^-$ compounds have shown that symmetrical supramolecular cations such as (K^+)([18]crown-6), Ca^{2+}([18]crown-6)$(CH_3CN)_2$, and Cs^+_2([18]crown-6)$_3$, with a C_3-axis through the center of the crown ether, normal to the molecular plane, possess a tendency to form antiferromagnetic $[Ni(dmit)_2]^-$ anion arrangements, such as a linear one-dimensional chain via lateral S···S interactions along the long axis, or π-dimers between the $[Ni(dmit)_2]^-$ anions. From the viewpoint of correlating between the structure and the magnetic properties, reducing the symmetry of the supramolecular cation may provide a ferromagnetic interaction between the $[Ni(dmit)_2]^-$ anions. Herein, we describe our studies involving supramolecular cations featuring a Cs^+ ion with benzo[18]crown-6 (B[18]crown-6) or dibenzo[18]crown-6 (DB[18]crown-6) as the counterion to the $[Ni(dmit)_2]^-$ anions (Scheme 1). The point group of the crown ether, C_s for B[18]crown-6 and C_{2v} for DB[18]crown-6, has been shown to influence the arrangement of the $[Ni(dmit)_2]^-$ anions within the crystals. The crystals of Cs^+_2(B[18]crown-6)$_3[Ni(dmit)_2]^-_2$ (**1**) and Cs^+(DB[18]crown-6)$_2[Ni(dmit)_2]^-$ (**2**) with different crystal stoichiometries were obtained. Among these crystals, the symmetry of the supramolecular assembly for Cs^+-B[18]crown-6 was lower than that for Cs^+-DB[18]crown-6. In the case of the $(Cs^+)_2$(B[18]crown-6)$_3$ supramolecule (salt **1**), the simultaneous control between the $J_F > 0$ and $J_{AF} < 0$ interactions was achieved for the different arrangements of the $[Ni(dmit)_2]^-$ anions.

Experimental Section

Preparation of [Ni(dmit)$_2$] Salts. The precursor monovalent (n-Bu_4N)$[Ni(dmit)_2]$ salt was prepared according to the literature.[12] Single crystals of salts **1** and **2** were obtained via the density gradient method in a vial cell (~50 mL). A green solution of (n-Bu_4N)$[Ni(dmit)_2]$ (20 mg) in CH_3CN (~20 mL) was slowly poured into a solution of $(Cs^+)(I^-)$ and B[18]crown-6 or DB[18]crown-6 (~200 mg) in CH_3CN (~30 mL) (detailed conditions of the single crystal preparation are listed in Supporting Information, Table S1). After 2 weeks, single crystals (typical dimensions: 0.4 × 0.4 × 0.3 mm) were obtained as black blocks. The stoichiometry of crystals was determined by X-ray structural and elemental analyses (Supporting Information, Table S2).

Table 1. Crystallographic Data of Salts **1** and **2**

	1	**2**
formula	$C_{30}H_{36}O_9S_{10}NiCs$	$C_{46}H_{48}O_{12}S_{10}NiCs$
F.W	1052.81	1305.08
crystal system	Triclinic	Monoclinic
space group	$P\bar{1}$ (No. 2)	$P2_1/c$ (No. 14)
crystal size, mm^3	0.30 × 0.20 × 0.10	0.40 × 0.30 × 0.10
a, Å	12.7899(7)	14.7024(5)
b, Å	13.0539(7)	24.1190(10)
c, Å	27.1703(15)	15.3970(5)
α, deg	78.3394(18)	
β, deg	77.0109(16)	100.8510(12)
γ, deg	70.6358(15)	
V, Å^3	4129.8(4)	5362.3(3)
Z	4	4
D_{calc}, g cm^{-3}	1.693	1.616
temperature, K	296	296
μ, cm^{-1}	18.92	14.78
no. of reflections measured	40252	79511
no. of independent reflections	18565	12191
no. of reflections used	18565	12191
R^a	0.0401	0.0366
$R_w{}^a$	0.1137	0.1098
GOF	1.038	1.077

[a] $R = \sum||F_o| - |F_c||/\sum|F_o|$ and $R_w = \{\sum[w(F_o^2 - F_c^2)^2]/\sum w(F_o^2)^2\}^{1/2}$.

X-ray Structural Analysis. Crystallographic data (Table 1) were collected using a Rigaku RAXIS-RAPID diffractometer using Mo Kα (λ = 0.71073 Å) radiation from a graphite monochromator. Structure refinements were carried out using the full-matrix least-squares method on F^2. Calculations were performed using Crystal Structure software packages.[13] Parameters were refined using anisotropic temperature factors, except for those of the hydrogen atom.

Magnetic Susceptibility. Temperature-dependent magnetic susceptibility and magnetization-magnetic field dependence were measured using a Quantum Design MPMS-XL5 SQUID magnetometer using polycrystalline samples. The applied magnetic field was 1 T for all temperature-dependent measurements. The magnetization-magnetic field ($M-H$) curve of salt **1** was measured under a maximum applied magnetic field of +5 T.

Calculation of Transfer Integrals. The transfer integrals (t) between the $[Ni(dmit)_2]^-$ anions were calculated within the tight-binding approximation using the extended Hückel molecular orbital method. The lowest unoccupied molecular orbital (LUMO) of the $[Ni(dmit)_2]^-$ molecule was used as the basis function.[14] Semiempirical parameters for Slater-type atomic orbitals were obtained from the literature.[14] The t values between each pair of the molecules were assumed to be proportional to the overlap integral (S) according to the equation $t = -10S$ eV.

Electron Spin Resonance. Temperature-dependent ESR spectra were measured using a JEOL JES FA-100 spectrometer equipped with a temperature control system (Oxford ESR900 cryostat). Single

(12) Steinmecke, G.; Sieler, H. J.; Krimes, R.; Hoyer, E. *Phosphorus Sulfur* **1979**, *7*, 49.

(13) (a) *Crystal Structure: Single crystal structure analysis software*, Ver. 3.6; Rigaku Corporation and Molecular Structure Corporation, 2004. (b) Sheldrick, G. M. University of Götingen, 1993/1997/2001.

(14) Mori, T.; Kobayashi, A.; Sasaki, Y.; Kobayashi, H.; Saito, G.; Inokuchi, H. *Bull. Chem. Soc. Jpn.* **1984**, *57*, 627.

Table 2. Transfer Integrals (t) between the [Ni(dmit)$_2$]$^-$ Anions and Magnetic Parameters of Salts **1** and **2**[a]

t, meV[a]	**1**	**2**	magnetism	**1**	**2**
t_1	2.7	2.8	coupling	F and AF	AF
t_2	1.1	1.4	C, emu K mol^{-1}	0.193 and 0.193[b]	0.375
t_3	12.3	0.1	θ or J, K	+1.1 and −5.2	−24.8
t_4	3.6				

[a] Transfer integrals were calculated from the LUMO of [Ni(dmit)$_2$] based on the extended Hückel calculation ($t = -10S$ eV, S is the overlap integral). The t_1−t_4 are specified in Figure 3 and 4. [b] The C was distributed at one-half for [Ni(dmit)$_2$]$^-$ **A** and **B** + **C**, respectively.

crystals were attached to a support on a quartz sample holder. The g-values of the ESR signals were corrected at the third and fourth reference signals of MnO. All ESR signals were fitted using the Lorentzian line shape.

Results and Discussion

As described above, the crystals of (Cs$^+$)$_2$(B[18]crown-6)$_3$[Ni(dmit)$_2$]$^-_2$ (**1**) and (Cs$^+$)(DB[18]crown-6)$_2$[Ni(dmit)$_2$]$^-$ (**2**) are composed of Cs$^+$-crown ether supramolecular assemblies and monovalent [Ni(dmit)$_2$]$^-$ anions. The crystal symmetry of salt **2** (monoclinic $P2_1/c$) was higher than that of salt **1** (triclinic $P\bar{1}$), while the crystal density of salt **2** (D_{calc} = 1.616 gcm^{-3}) was lower than that of salt **1** (D_{calc} = 1.693 gcm^{-3}). For both salts, the monovalent electronic structure of the [Ni(dmit)$_2$]$^-$ anions (S = 1/2) was confirmed using their electronic absorption spectra (Supporting Information, Figure S4), which exhibited a broad absorption maximum around 9 × 10^3 cm^{-1}. The t values and magnetic properties of salts **1** and **2** are summarized in Table 2. Although the recent progress of symmetry-broken density functional theory (DFT) calculations enable us to predict the sign of J for the dmit-based molecules,[15] the transfer integral (t) based on the extended Hückel molecular orbital calculation is a simple structural parameter to estimate the magnitude of the $|J|$ according to the equation of $|J| \sim 4t^2/U_{eff}$, where U_{eff} is the effective on-site Coulomb repulsive energy of the [Ni(dmit)$_2$]$^-$ anions.[16]

Structures of the Supramolecular Cations. The six oxygen atoms of both B[18]crown-6 and DB[18]crown-6 possess the ability to establish the location of the Cs$^+$ ion via Cs$^+$···O interactions.[17] Because the Cs$^+$ ionic radius (∼1.69 Å) is larger than the cavity radius of [18]crown-6 (1.3−1.6 Å), a dodeca-coordinated sandwich-type Cs$^+$([18]crown-6)$_2$ or a club-sandwich-type Cs$^+_2$([18]crown-6)$_3$ assemblies was formed.[17,18] In the case of salt **1**, the club-sandwich-type Cs$^+_2$(B[18]crown-6)$_3$ supramolecule was observed, with an average Cs$^+$···O distance of 3.32 Å (Figure 2a), which is similar to that observed for (Cs$^+$)$_2$([18]crown-6)$_3$[Ni(dmit)$_2$]$^-_2$.[11e] Because each crystallographically independent unit involves two Cs$^+$ ions and three B[18]crown-6 molecules, an inversion center did not exist for the Cs$^+_2$(B[18]crown-6)$_3$ supramolecular cation. The alternate arrangement of the benzene rings of B[18]crown-6 avoided steric hindrance between the nearest neighbor B[18]crown-6 in the triad assembly. The lack of an inversion center within the assembly reduced the symmetry of the supramolecule and the packing structure. In the case of salt **2**, the jack-knife-shaped DB[18]crown-6 molecules stacked via dodeca-coordination between the Cs$^+$ ion and the oxygen atoms of DB[18]crown-6 (Figure 2, panels b and d), where the average Cs$^+$···O distance of 3.32 Å was similar to that of salt **1**. The surface potential of the overall cationic structures of salts **1** and **2** are shown in Figure 2c,d. The symmetry of Cs$^+$(DB[18]crown-6)$_2$ was higher than that of Cs$^+_2$(B[18]crown-6)$_3$ and affected the packing structures in salts **1** and **2**.

Packing Structures for Salts 1 and 2. The packing structures of the cations and anions for salt **1** are summarized in Figure 3. Alternating layers of the Cs$^+_2$(B[18]crown-6)$_3$ cations and [Ni(dmit)$_2$]$^-$ anions were extended along the c-axis (Figure 3a). As shown in Figure 3b, the Cs$^+_2$(B[18]crown-6)$_3$ cations stacked along the a-axis. Between the cation layers, two different arrangements of the [Ni(dmit)$_2$]$^-$ anions were observed. A single crystallographically independent unit can be defined using the halves of two [Ni(dmit)$_2$]$^-$ anions (**A** and **B**) and one [Ni(dmit)$_2$]$^-$ anion (**C**), in which the inversion centers are located on the Ni atom of the **A** and **B** anions. The **A** and **B** anions formed a two-dimensional layer via lateral S···S contacts along the a-b and b-axis (Figure 3c), whereas the **C** anions formed a one-dimensional π-dimer chain along the a-axis (Figure 3d). The **A**−**B** layer involved an alternating ···**A**···**B**···**A**···**B**··· arrangement via lateral S···S contacts along the short axis of the [Ni(dmit)$_2$]$^-$ anion along the a-axis, with a transfer integral of $t_1 \sim$ 2.7 meV for each anion. In addition to the t_1-interaction, a t_2-interaction of ∼1.2 meV was observed along the a-b axis, which is the basis for the two-dimensional [Ni(dmit)$_2$]$^-$ layer within the ab-plane.

In contrast to the two-dimensional layer of the **A** and **B** anions, the packing arrangement of the **C** anions was completely different. The **C** anions formed π-dimers with an intradimer t_3 interaction of ∼ 12.3 meV, with additional lateral S···S t_4 interactions of ∼ 3.6 meV along the a-axis. Because the π-dimer is surrounded by four Cs$^+_2$(B[18]crown-6)$_3$ supramolecules, each dimer chain is isolated from each other. In salt **1**, the coexistence of two arrangements of the [Ni(dmit)$_2$]$^-$ anions was achieved and can be attributed to the lower symmetry of the Cs$^+_2$(B[18]crown-6)$_3$ supramolecular cations than that of the Cs$^+_2$(DB[18]crown-6)$_2$ cations.

The packing structures of the cations and anions for salt **2** are summarized in Figure 4, in which a crystallographically independent unit is defined by one [Ni(dmit)$_2$]$^-$ anion **A**. In contrast to that of the Cs$^+_2$(B[18]crown-6)$_3$ cation, the higher symmetry of the Cs$^+$(DB[18]crown-6)$_2$ assembly yielded a simpler packing arrangement of the [Ni(dmit)$_2$]$^-$ anions than

(15) See references in (a) Cauchy, T.; Ruiz, E.; Jeannin, O.; Nomura, M.; Fourmigué, M. *Chem.—Eur. J.* **2007**, *13*, 8858. (b) Grosshans, P.; Adkine, P.; Sidorenkova, H.; Nomura, M.; Fourmigué, M.; Geoffroy, M. *J. Phys. Chem. A* **2008**, *112*, 4067.

(16) Scott, J. C. *Semiconductor and Semimetals. High Conducting Quasi-One-Dimensional Organic Crystals*; Conwell, E. Ed.; Academic Press: New York, 1988; p 385.

(17) (a) Weber, E.; Toner, J. L.; Goldberg, I.; Vögtle, F.; Laidler, D. A.; Stoddart, J. F.; Bartsch, R. A.; Liotta, C. L. *Crown ethers and analogs*; Patai, S.; Rappoport, Z., Eds.; John Wiley & Sons: New York, 1989. (b) Gokel, G. W. *Crown Ethers & Cryptands*; Stoddart, J. F., Ed.; RSC: Cambridge, 1994.

(18) Vidal, J. L.; Schoening, R. C.; Troup, J. M. *Inorg. Chem.* **1981**, *20*, 227.

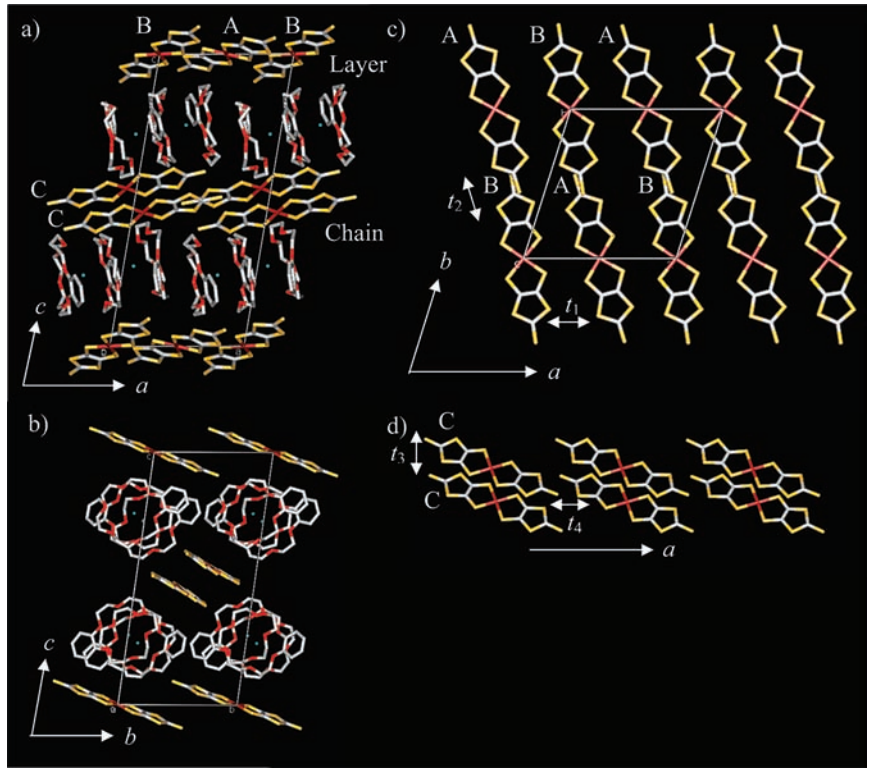

Figure 3. Crystal structures of salt **1**. Unit cell viewed along the *b*-axis (a) and *a*-axis (b). Arrangements of the $[Ni(dmit)_2]^-$ anions in the two-dimensional **A**···**B** layer (c) and one-dimensional π-dimer chain of **C** (d). Intermolecular transfer integrals (t_1-t_4) are illustrated.

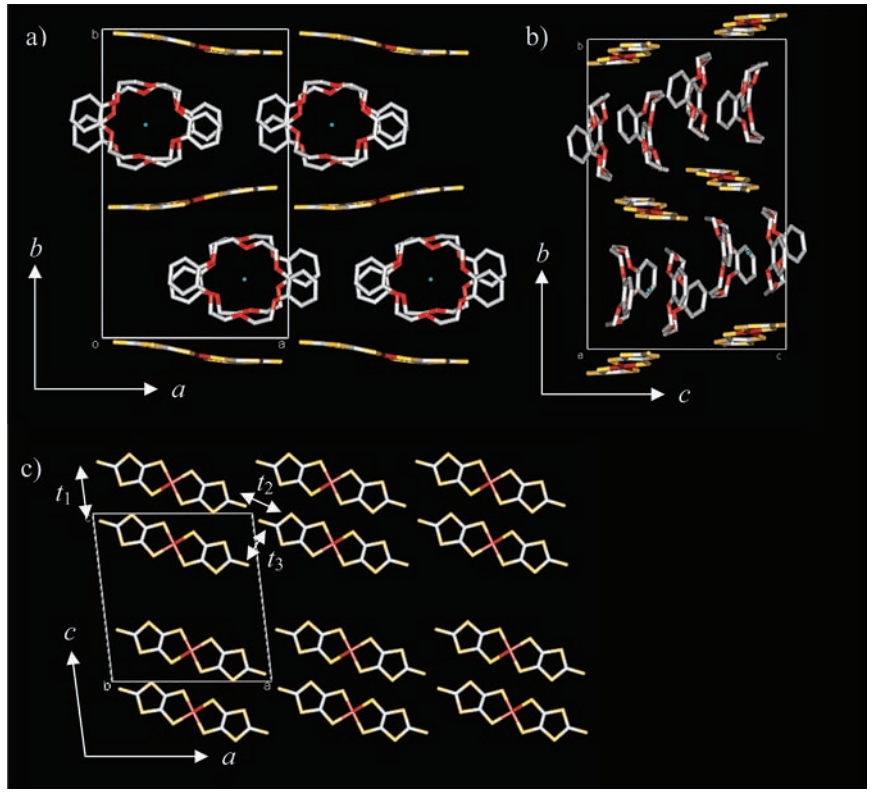

Figure 4. Crystal structure of salt **2**: The unit cell viewed along the *c*-axis (a) and *a*-axis (b), and the arrangement of the $[Ni(dmit)_2]^-$ anions in the *ac*-plane (c). Intermolecular transfer integrals (t_1-t_3) are illustrated.

that for salt **1**. The alternating arrangements of the Cs^+ $(DB[18]crown\text{-}6)_2$ cations and the $[Ni(dmit)_2]^-$ anions extended along the *b*-axis (Figure 4, panels a and b). Effective interatomic interactions between the supramolecular cations and the $[Ni(dmit)_2]^-$ anions, within the limits of van der Waals contacts, were not detected. The $[Ni(dmit)_2]^-$ anions formed lateral dimers along their short axis with a t_1 interaction of ~2.8 meV. Furthermore, weak lateral S···S

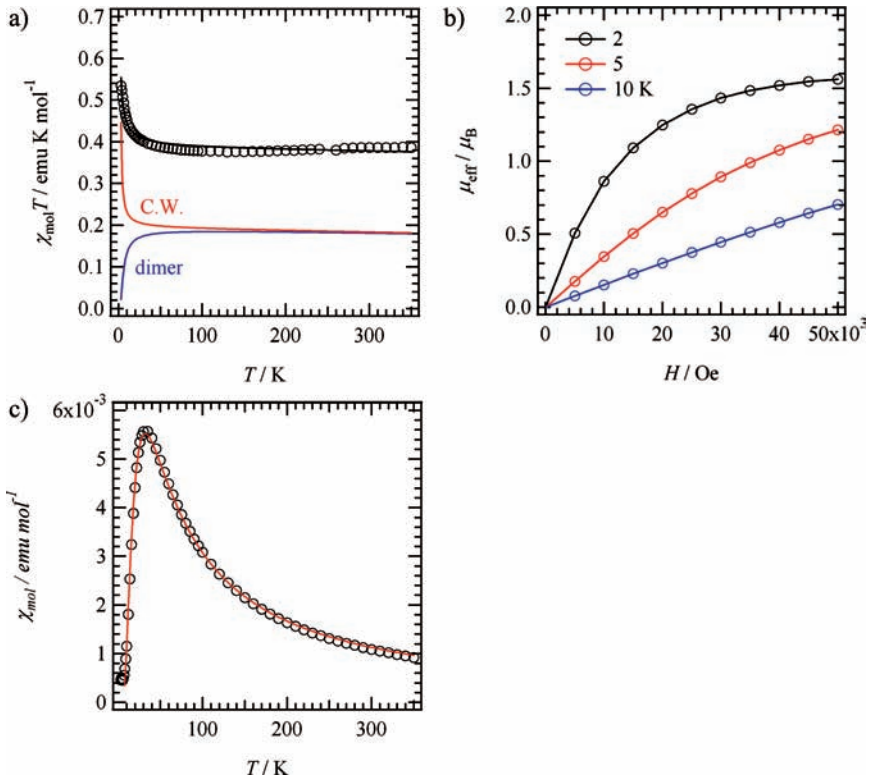

Figure 5. Temperature dependent molar magnetic susceptibility (χ_{mol}) of salts **1** and **2** per one [Ni(dmit)$_2$]$^-$ anion. (a) The $\chi_{mol}T$ vs T plots of salt **1**. The $\chi_{mol}T$ was divided into the two components of the Curie−Weiss model with a positive J_F (red line) and a dimer model (blue line). The combination of both models is indicated as the black line in the $\chi_{mol}T$ vs T plots. (b) Effective magnetic moment (μ) vs magnetic field (H) dependence of salt **1** at 2 (black), 5 (red), and 10 K (blue). (c) The χ_{mol} vs T plots of salt **2**. Best fit using the dimer model (red line).

contacts ($t_2 \sim 1.4$ and $t_3 \sim 0.1$ meV) along the long axis of the [Ni(dmit)$_2$]$^-$ anions yielded the one-dimensional dimer chain along the *a*-axis. Because the Ni···Ni distance between the nearest neighbor along the *c*-axis was longer than 10 Å, the dimer chains were isolated from each other along the *c*-axis. According to this arrangement of the [Ni(dmit)$_2$]$^-$ anions, the directions of the t_1- and t_2-interactions are not parallel to each other and, therefore, a linear magnetic chain was not formed along the *a*-axis.

Magnetic Properties. The temperature dependent magnetic susceptibilities (χ_{mol}) were significantly different between salts **1** and **2**. In the case of salt **1**, two types of magnetic interactions coexisted. As shown in Figure 3d, the intradimer interaction between the **C** dimer ($t_3 = 12.3$ meV) was 3-fold that of the interdimer interaction ($t_4 = 3.6$ meV). Therefore, the J within the **C** dimer should be antiferromagnetic interaction with $J < 0$. In the two-dimensional layer of the **A** and **B** anions, the transfer integrals along the *a*-axis ($t_1 = 2.7$ meV) was twice that along the *a*-*b* axis ($t_2 = 1.1$ meV). As shown in Figure 5a, the $\chi_{mol}T$ versus T behavior of salt **1** followed the Curie−Weiss law with a Curie constant of 0.375 emu K mol^{-1} over a temperature range of 50 to 350 K. According to these results, therefore, every one of the [Ni(dmit)$_2$]$^-$ anions (**A**, **B**, and **C**) contributed to the magnetic property of salt **1** at room temperature. It is important to note that the enhanced $\chi_{mol}T$ values below 50 K corresponded to the ferromagnetic interactions in salt **1**. The magnetic field (H) versus magnetization (M) curve at 2 K was in agreement with the ferromagnetic coupling of $S = 1/2$ spin, while the effective magnetic moment of about 1.6 μ_B at the applied magnetic field of 5 T was almost consistent with ideal $S = 1/2$ spin (1.73 μ_B with $g = 2$). Temperature dependent alternating current (AC) susceptibility measurements, however, did not indicate any ferromagnetic ordering above 2 K. The $\chi_{mol}T$ versus T behavior of salt **1** can be explained using a combination of the Curie−Weiss model, with ferromagnetic interaction for the **A**−**B** layer (red line in Figure 5a), and the dimer model, for the **C** anions (blue line in Figure 5a), as defined in (eq 1),

$$\chi_{mol} = 0.5\chi_{A-B} + 0.5\chi_C \quad (1)$$

The Curie constants for each unit (χ_{A-B} and χ_C) were defined as 0.193 emu K mol^{-1} for the Cs$^+$(B[18]crown-6)$_{1.5}$[Ni(dmit)$_2$]$^-$ salt. The $\chi_{mol}T$ versus T behavior was highly reproducible using a Weiss temperature (θ) of + 1.1 K for the **A**−**B** layer and $J = -5.2$ K for the **C** dimer. The weak lateral intermolecular interactions of t_1 and t_2 within the **A**−**B** layer should be important to yield the ferromagnetic magnetic interaction with the $J > 0$.

As shown in Figure 5c, the χ_{mol} versus T plot of salt **2** exhibited a broad maximum at ~30 K, which is typical for antiferromagnetic dimers or one-dimensional antiferromagnetic Heisenberg chains. The intermolecular interaction within a lateral [Ni(dmit)$_2$]$^-$ dimer ($t_1 \sim 2.8$ meV) was twice that between two dimers (interdimer, $t_2 \sim 1.4$ meV). Assuming $J \sim 4t^2$, the intradimer J_1/interdimer J_2 ratio should be 4:1. Because the directions of the t_1- and t_2-interactions are not parallel to each other, the one-dimensional chain model was inadequate to explain the χ_{mol} versus T behavior of salt **2**. Consequently, the dimer model was employed to

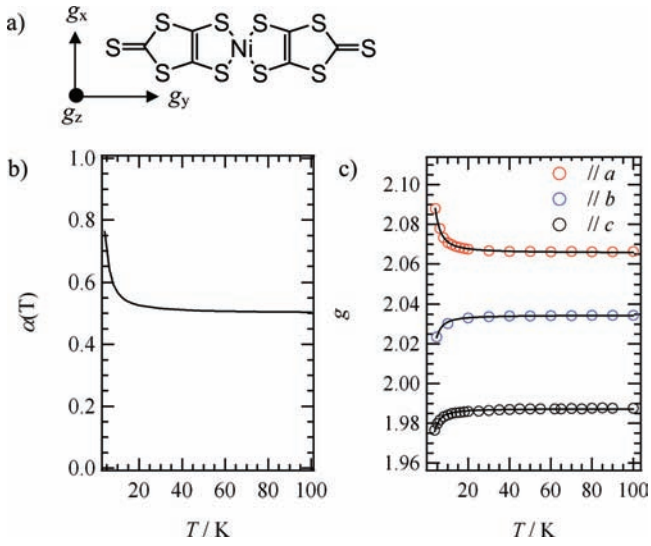

Figure 6. Temperature-dependent g values of the ESR spectra of salt **1**. (a) Principal g_x and g_y tensors are along the short and long axis of the anion, whereas the g_z tensor of $[Ni(dmit)_2]^-$ was normal to the π-plane. (b) Calculated temperature-dependent $\alpha(T)$ in eq 2. (c) g vs T plots of the single crystal. The magnetic fields were applied along the a- (red), b- (blue), and c-axis (black) of the single crystal. Best fit lines were calculated using the eq 3 (solid line).

explain the χ_{mol} versus T behavior, which is in accordance with the Curie constant of 0.193 emu K mol^{-1} and $J = -24.8$ K (red line in Figure 5c). Magnetic interactions within salt **2** was dictated by the antiferromagnetic dimer via lateral S···S contacts between the $[Ni(dmit)_2]^-$ anions.

The magnetic behavior of salt **1** was further investigated using temperature-dependent g values given by the electron spin resonance (ESR) spectra. The magnetic susceptibility of salt **1** was explained using two types of magnetic interactions: (a) ferromagnetic coupling (χ_{A-B}) in the **A**−**B** layer, and (b) antiferromagnetic coupling (χ_C) in the **C** dimer. Lowering of the temperature enhanced the χ_{A-B} (from the spin-only value), whereas the opposite temperature-dependency was observed for χ_C. The temperature-dependent contributions from χ_{A-B} toward the overall magnetic susceptibility ($\chi_{A-B} + \chi_C$) can be defined as[19,20]

$$\alpha(T) = \chi_{A-B}/(\chi_{A-B} + \chi_C) \quad (2)$$

As shown in Figure 6b, at room temperature, a value of 0.5 for $\alpha(T)$ corresponds to equal contributions from χ_{A-B} and χ_C. Below 20 K, values for $\alpha(T)$ increased with lower temperatures, reaching $\alpha(T) \sim 0.75$ at 4 K. The temperature-dependent anisotropic g values of the single crystal can be explained using $\alpha(T)$ and molecular arrangements in the crystal (Figure 6c). Noteworthy anisotropic behaviors of the g values were observed for the g (//a) versus T, g (//b) versus T, and g (//c) versus T plots. The absolute magnitude of these g values increased according to the axes, in the order of a- > b- > c-axis. Notably, the temperature-dependency of the g values along the a-axis (enhanced by lowering the temperature) was opposite those along the b- and c-axes. Such temperature-dependences can be explained by the anisotropy of the g factors of the $[Ni(dmit)_2]^-$ anions and the parameter of $\alpha(T)$. Because the principle g_x and g_y tensors were assigned along the short and long axes of the $[Ni(dmit)_2]^-$ anion, the g_z tensor was normal to the π-plane of the $[Ni(dmit)_2]^-$ anion (Figure 6a). The value for g_x (~2.09) was slightly larger than that for g_y (2.03) and g_z (2.00).[21] For the crystal structure of salt **1**, the short axes of the **A** and **B** anions (g_x direction) were nearly in alignment with the a-axis, whereas the long axis (g_y direction) of the **C** anion was aligned with the a-axis. The g (//a) versus T behavior (Figure 6c), which is assisted from g_x of the **A** and **B** anions and g_y of **C** anion, can be defined along the a-axis as

$$g(T) = \alpha(T)g_x + [1 - \alpha(T)]g_y \quad (3)$$

which can be fitted using $g_x = 2.11$ and $g_y = 2.02$ (solid line in Figure 6c); the direction of the a-axis, however, was not precisely consistent with the direction of g_x and g_y. Along the b-axis, g_y for the **A** and **B** anions and g_x for the **C** anion contributed to the g (//b) versus T behavior, in which the contribution from g_x was suppressed by a factor of $\alpha(T) - 1$. As shown in Figure 6c, the g (//b) versus T plots can also be reproduced as a best fit plot. Because the π-planes of the $[Ni(dmit)_2]^-$ anions (**A**, **B**, and **C**) are inclined at about 30° from the ab-plane, both g_z and g_y contribute to the g (//c) versus T plots, which can be reproduced using $g_y = 2.01$ and $g_z = 1.97$.

Conclusions

Benzo[18]crown-6 (B[18]crown-6) and dibenzo[18]crown-6 (DB[18]crown-6) were complexed with Cs^+ ions, forming the sandwich-type Cs^+_2(B[18]crown-6)$_3$ and Cs^+(DB[18]crown-6)$_2$ supramolecular cations, which were then introduced as counterions to $[Ni(dmit)_2]^-$ anions to yield Cs^+_2(B[18]crown-6)$_3$$[Ni(dmit)_2]^-_2$ (**1**) and Cs^+(DB[18]crown-6)$_2$$[Ni(dmit)_2]^-$ (**2**) salts. The crystal structures of both salts consisted of alternating layers of supramolecular cations and $[Ni(dmit)_2]^-$ anions, in which the arrangements of the $[Ni(dmit)_2]^-$ anions determined the intermolecular magnetic exchange energy (J) between the $S = 1/2$ spins on the $[Ni(dmit)_2]^-$ anions. In salt **1**, a two-dimensional layer via lateral S···S contacts between the $[Ni(dmit)_2]^-$ anions (**A** and **B**) and a π-dimer chain of the $[Ni(dmit)_2]^-$ anions (**C**) were observed. The temperature-dependent magnetic susceptibility of salt **1** was reproduced using two components of the dimer model, with $J = -5.2$ K, and ferromagnetic coupling, with $J = +1.1$ K. The anisotropic temperature-dependent g factors of the single crystal also supported the independent contribution from the two-dimensional layer and the dimer. In salt **1**, magnetic interactions with ferromagnetic ($J > 0$) and antiferromagnetic ($J < 0$) coupling was shown to coexist, corresponding to the

(19) Mukai, K.; Senba, N.; Hatanaka, T.; Minakuchi, H.; Ohara, K.; Taniguchi, M.; Misaki, Y.; Hosokoshi, Y.; Inoue, K.; Azuma, N. *Inorg. Chem.* **2004**, *43*, 566.
(20) (a) Tomkiewicz, Y.; Taranko, A. R.; Torrance, J. B. *Phys. Rev. Lett.* **1976**, *36*, 751. (b) Takahashi, M.; Sugano, T.; Kinoshita, M. *Bull. Chem. Soc. Jpn.* **1984**, *57*, 26.
(21) (a) Mukai, K.; Shiba, D.; Yoshida, K.; Mukai, K.; Hisatou, H.; Ohara, K.; Hosokoshi, Y.; Azuma, N. *Bull. Chem. Soc. Jpn.* **2005**, *78*, 2114. (b) Nakamura, T.; Takahashi, T.; Aonuma, S.; Kato, R. *J. Mater. Chem.* **2001**, *11*, 2159.

A−**B** layer and **C** dimer of [Ni(dmit)$_2$]$^-$ anion arrangements. In contrast, the symmetrical Cs$^+$(DB[18]crown-6)$_2$ cation yielded a lateral [Ni(dmit)$_2$]$^-$ dimer via interatomic S···S contacts, in which the magnetism can be explained using the dimer model with antiferromagnetic coupling. The arrangement of the [Ni(dmit)$_2$]$^-$ anions, along with the corresponding magnetism, was affected by the overall symmetry of the supramolecular cations. Our supramolecular methodology, which can offer the coexistence of positive and negative magnetic coupling within a crystal using asymmetrical supramolecular cations, can afford novel magnetic exchange interactions.

Acknowledgment. This work was partly supported by a Grant-in-Aid for Science Research from the Ministry of Education, Culture, Sports, Science, and Technology of Japan. T.A. thanks the Murata Science Foundation for financial support.

Supporting Information Available: The atomic numbering scheme, structural analysis of salts **1** and **2**, vibrational spectra, electronic spectra in KBr pellets, Raman spectra, and ESR spectra of salt **1**. This material is available free of charge via the Internet at http://pubs.acs.org.

IC9001847